A Comprehensive Study of the Effect of Thermally Induced Surface Terminations on Nanodiamonds Electrical Properties

CORRECTIVE ALGORITHMS FOR MEASUREMENT IMPROVEMENT IN MScMS-II (MOBILE SPATIAL COORDINATE MEASUREMENT SYSTEM)*

GALETTO MAURIZIO, MASTROGIACOMO LUCA

Dipartimento di Sistemi di Produzione ed Economia dell'Azienda, Politecnico di Torino, C.so Duca degli Abruzzi 24, Torino, 10129, Italy
e-mail: maurizio.galetto@polito.it

Abstract

This paper presents a set of algorithms for the correction of measurement errors of a prototype system designed for Large Scale Dimensional Metrology (LSDM) applications. The system, developed in the Quality and Industrial Metrology Laboratory of Politecnico di Torino, is based on the principles of photogrammetry and consists of a set of cameras wirelessly connected to a central unit able to track the position of a portable contact probe. Due to its architecture the system is affected by several systematic error sources. This paper addresses some of them: the distortion of the lenses, the dimension of the probe tip and the kinematic of the probe. By means of the implementation of appropriate mathematical correction models, the overall system performance is significantly improved as shown by the conducted tests.

***Keywords*:** Large Scale Dimensional Metrology, MScMS, lens distortion, Kalman Filter, probe tip correction.

1. Introduction

Nowadays, one of the most challenging issues for coordinate metrology instruments is to ensure consistent performance throughout the whole working volume. This goal is even tougher in the field of Large Scale Dimensional Metrology (LSDM) when the dimensions of the working volumes are of the order of several meters (Franceschini, Galetto et al. 2011; Hocken and Pereira 2012). Distributed measurement systems, which are characterized by a distributed hardware architecture based on a network of metrology stations spread in a well defined working volume, seem to particularly suffer this problem (Galetto, Mastrogiacomo et al. 2010). With particular regards to this type of system, several corrective models have been proposed in order to partially address this issue. Some of them are already integrated into the onboard firmware and software applications. This paper deals with the algorithms for error correction implemented into a new prototype system developed at Politecnico di Torino, the Mobile Spatial coordinate Measurement System (MScMS-II) (Galetto, Mastrogiacomo et al. 2011). Relying on the principles of close-range photogrammetry, the system is able to define the position of its probe and, as a consequence, to reconstruct the measured geometries (Luhmann, Robson et al. 2006). Because of its architecture and working principle, the system is affected by several error sources that impact differently on system performance (Galetto, Mastrogiacomo et al. 2010). The distortion of each camera lens, as well as the physical size of the probe that can approach the measurand with different trajectories, but also the kinematics of the probe are just some of the factors that can cause bias and variability during the

* This work and the whole research program "Large-scale coordinate metrology: study and realization of an innovative system based on a network of distributed and cooperative wireless sensors" (PRIN 2008) have been financially supported by the Italian Ministry of University and Scientific and Technological Research (MIUR).

measurement (Bar-Shalom, Li et al. 2001; Luhmann, Robson et al. 2006). This paper aims at analyzing the different error factors verifying their impacts by proposing some correction models addressed at the improvement of the global metrological performance of the system. For each of the models presented in the paper, a discussion about its implementation is given along with some preliminary results in terms of performance improvement.

2. About MScMS-II

The MScMS-II (Mobile Spatial coordinate Measuring System) is a prototype system designed for large scale metrology applications. It is characterized by a distributed modular architecture, consisting of a network of wireless sensing devices, a remote portable and armless probe, and a centralized data processing unit (Fig. 1). The network consists of a set of infrared (IR) cameras, that communicate to the data processing unit, through a wireless Bluetooth link, the information related to the spatial positioning of two reference markers embedded on the portable probe. Low-cost IR cameras, characterized by an interpolated resolution of 1024x768 pixels, a maximum sample rate of 100 Hz, and an angular Field-Of-View (FOV) of approximately 45°×30°, have been chosen as sensor network devices (Lee 2008). Since passive tracking has been implemented, each sensor is coupled with a near-IR light source (IR LED array) to properly illuminate the working volume and hence making retro-reflective markers visible in the camera field-of-sensing. The overall sensor set (camera and LED array, see Fig. 2) weighs about 500 g and is 13×13×15 cm in size.

Figure 1. MScMS-II prototype. (a) Sensor network configuration: black circles highlight the spatial position of the network nodes.

Each camera is provided with an embedded real-time tracking engine, which is in charge of image processing and filtering and determines the 2D coordinates of up to four the IR spot(s) in the camera view plane. To prevent noisy measurements and to filter undesired reflections, each network device only tracks

the brighter IR sources (Lee 2008) while no filtering on the shape of the light sources is performed. The capability of distributed computing significantly saves DPU computational effort. In this way, it is possible to add network devices without compromising the overall efficiency of the system in terms of operating speed.

The portable probe (see Fig. 2) is a rigid body, which consists of a set of two retro-reflective spherical markers and a contact tip to touch the measured object. The probe, realized in rapid prototyping, was calibrated by means of a CMM.

The data processing unit is in charge of gathering the data acquired from each sensing device, and processing them to provide 3D coordinates of markers and thus to localize the probe tip. Tip coordinates are then used in a post-processing phase to perform geometry reconstruction tasks (Galetto, Mastrogiacomo et al. 2010).

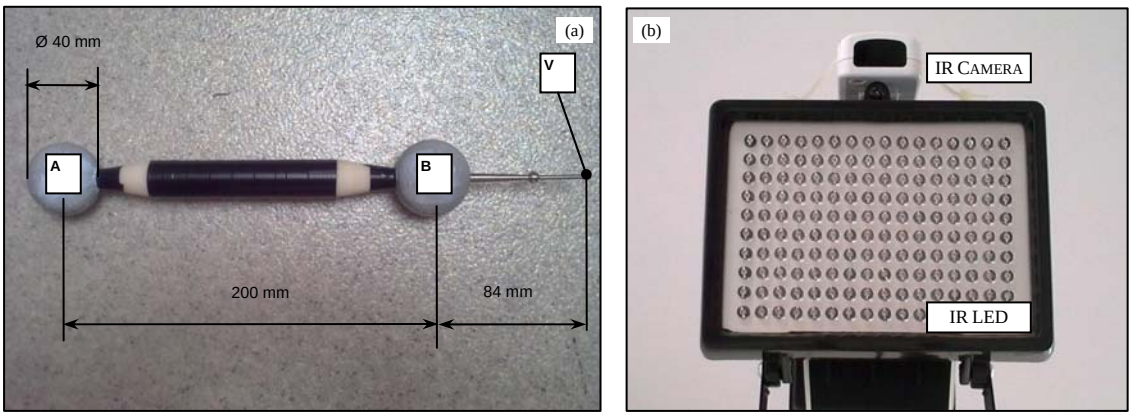

Figure 2. (a) Portable hand-held probe: A and B identify the retro-reflective markers whereas V is the contact point of the probe tip. (b) Main components of the IR-based sensor network: an IR camera is coupled with an IR LED array to locate passive retro-reflective targets.

The novelty of such a system can be mainly identified in its distributed architecture: the fact of consisting of a number of devices greater than strictly necessary allows the system to operate even in critical conditions, i.e. when some devices are not properly working because of breakdowns, malfunctions or simply because of shade effects due to the presence of the operator. The minimum number of devices for a proper functioning of the system is two. Some previous experiments showed the trend of the performance in one point of the working volume varying the number of devices involved in the localization (Franceschini, Galetto et al. 2011). The test was done by measuring a distance, whose nominal value is known (about 400 mm) in static conditions. The results, presented in Fig.3, show how the number of devices asymptotically affects the performance of the system.

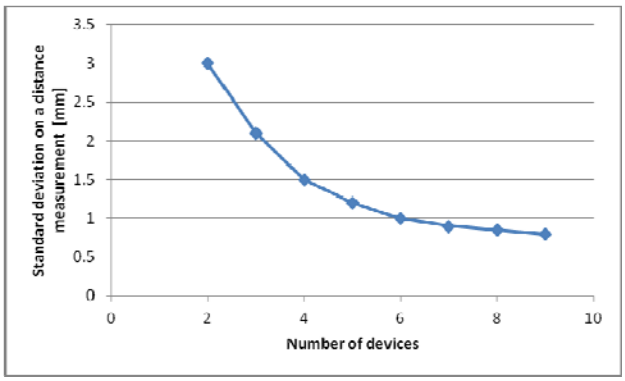

Figure 3. Assessment of MScMS-II performances varying the number of system devices.

The system in its current form is still a prototype under study. It was chosen to deliberately use low-cost hardware in its implementation to focus on software development. This paper is born from the effort to limit some of the errors due to the limitations of the technology used. Three different kinds of measurement errors (respectively due to the lens distortion, the probe physical size and its kinematics during measurement) are analyzed and corrected. All the tests proposed for the evaluation of the effect of each correction are performed with the prototype described above arranged in a layout of 3x3x2 m^3.

3. Lens distortion

Radial (symmetric) distortion constitutes the major imaging error for most camera systems. It is attributable to variations in refraction at each individual component lens within the objective. It is a function not only of the lens design used but also of the chosen focusing distance, and of the object distance at a constant focus. Fig. 4 shows the effect of radial distortion as a function of the image radius of an imaged point. In the example, the distortion increases with the distance from the principal point. For standard lenses radial distortion can reach more than 100 µm in the image corners. Brown (1971) shows that the distortion curve can be modeled with a polynomial series (Seidel series) with distortion parameters k_0 *to* k_n:

$$\begin{aligned} \Delta u_{rad} &= u(k_1 r^2 + k_2 r^4 + k_3 r^6 + \cdots) \\ \Delta v_{rad} &= v(k_1 r^2 + k_2 r^4 + k_3 r^6 + \ldots) \end{aligned} \qquad (1)$$

where u, v are the normalized pixel coordinates of a camera and $r = \sqrt{u^2 + v^2}$ (Brown 1971).
For most lens types the series can be truncated after the second or third term without any significant loss of accuracy.

Radial-asymmetric distortion, often called tangential or decentring distortion (Fig. 4), is another important imaging error, which is mainly caused by lack of concentricity and misalignment of individual lens elements within the objective. It can be compensated for by the following function (Brown 1971):

$$\begin{aligned} \Delta u_{tan} &= b_1(r^2 + 2u^2) + 2b_2uv \\ \Delta v_{tan} &= b_2(r^2 + 2v^2) + 2b_1uv \end{aligned} \qquad (2)$$

where b_1 and b_2 are tangential distortion coefficients. Compared to the radial-symmetric part, radial asymmetric distortion shows much smaller values for most quality lenses (Zhang 1999). Hence, it is often determined for high accuracy specifications only. In case of low cost lenses, significant tangential distortion can be found. For this reason, it is reasonable to expect a significant improvement in the performance of MScMS-II from the implementation of a correction model for both radial and tangential distortion. The complete correction model can be stated as:

$$\begin{aligned} u_{corrected} &= u + \Delta u_{rad} + \Delta u_{tan} \\ v_{corrected} &= v + \Delta v_{rad} + \Delta v_{tan} \end{aligned} \qquad (3)$$

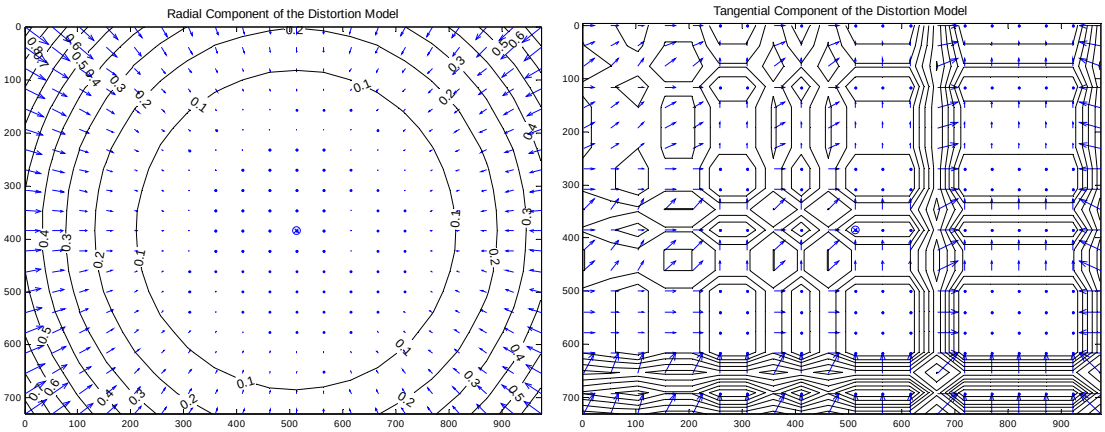

Figure 4. Lens distortion. (a) Example of lens radial distortion (b) Example of lens tangential distortion.

Fig. 4 presents an example of lens distortion correction. For each region of the image, the arrows indicate the direction and the magnitude of vectors $[\Delta u_{rad}; \Delta v_{rad}]$ and $[\Delta u_{tan}; \Delta v_{tan}]$ respectively.

3.1. *Test*

In order to verify the effectiveness of the proposed model, the following test was performed (Peggs, Maropoulos et al. 2009). A reference artifact was calibrated using a Coordinate Measuring Machine whose nominal accuracy is of the order of a hundredth of a millimeter (CMM – DEA Iota0101). Fig. 5 shows the reference artifact used for the experiment. On the artifact four different reference distances of about 100, 200, 400 and 500 mm were defined. The reference artifact was then measured in three different positions within the measuring volume of MScMS-II.

Figure 5. A photo of the reference artefact.

For each position of the reference artifact, the distances were measured with MScMS-II, replicating the measurements 10 times (for a total of 120 measurements). The results of these measurements with and without the correction of lens distortion were compared in terms of deviation from nominal values.

As expected, the performance of the system seems to improve with the distortion correction (see Fig. 6). The improvement is significant both in terms of bias and in terms of dispersion of the error distribution.

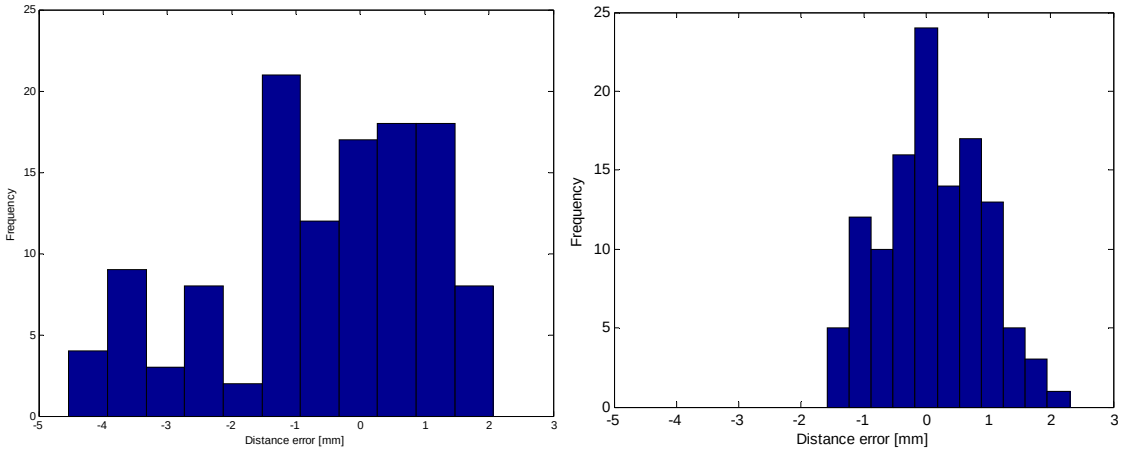

Figure 6. The effect of lens distortion correction. (a) Results of raw measurements (b) Results of corrected measurements.

In order to quantify the improvement, Table 1 shows the sample mean and the standard deviation of the error distribution with and without the correction model.

Table 1. Sample mean and standard deviation of error distribution.

	Without Correction	With Correction
Mean [mm]	-0.57	0.09
Standard deviation [mm]	1.61	0.82

A remarkable aspect that emerges from the proposed test is how the correction model changed the shape of the error distribution. The shape of the empirical distribution of corrected measurements shows to be much more symmetrical than the uncorrected one.

In order to verify the robustness of the obtained results, the test was repeated with the same and with different sensor locations, producing similar results.

These results justify the choice of this type of camera: despite the low resolution (native resolution is 128 x 996 pixels) the dispersion of the localization results is relatively low and comparable to what could be achieved with cameras with a higher resolution (640 x 480) which have significantly higher costs. Consider that the cost of an industrial camera with VGA resolution is currently higher than 400 €, while the cost of the devices used in the prototype is about 40 € each.

4. Bias due to the physical size of the probe

A problem common to all contact measuring instruments is the size of the tip of the probe which may introduce a bias in the contact measurement. For this reason, CMMs software typically implement some algorithms able to correct the measurement results taking into consideration the direction of the approach of the probe and the surface shape to be measured (Wozniak, Mayer et al. 2009).

The stylus tip radius correction (see Fig. 7) is an offset vector of norm equal to the effective stylus tip radius which is added to the indicated measured point (i.e. the measured stylus tip centre point) to estimate the actual contact or measured point on the profile (i.e. the stylus tip contact point on the actual surface). The nature of the tangential contact between a sphere and a surface results in the offset vector being normal to the surface at the point of contact so the primary task for correction is to estimate this vector for each data point. In the case of a freeform surface or for a contour, the measuring surface normal vector can be unknown especially when dealing with measurements of tight radii, corners or discontinuities in general. A number of approaches have been proposed for solving this problem (Wozniak, Mayer et al. 2009).

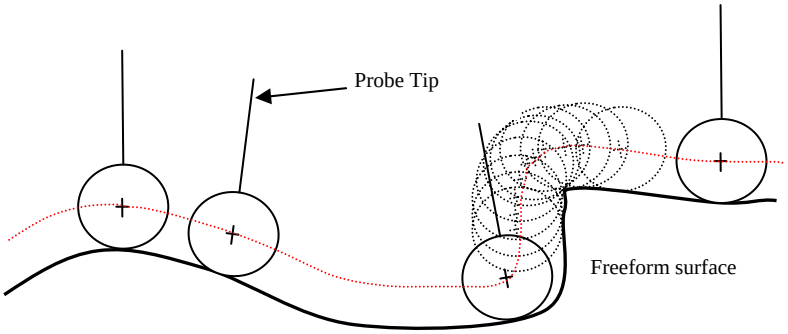

Figure 7. A schematization of the stylus tip approach to a free form. The dotted line represents the envelop of the points measured by the CMM which do not exactly correspond to the surface to be measured. This is particularly evident in case of angular points.

Many methods use a set of measured points to estimate the direction of correction. Most of the methods use NURBS or cubic splines to obtain a best fit curve through the measured point and its normal vectors in order to compensate as a post-measurement operation. Such a scheme, for example, is proposed by Zhongwei et al. (Zhongwei, Yuping et al. 2003). Another solution assumes that in the neighbourhood of the measured point, the surface may be approximated by a quadratic equation (Song and Kim 1997). Mayer et al. also used the measured points to fit the surface generated by the stylus tip centre and then finding the corresponding normal vector (Mayer, Mir et al. 1997). On the other hand, Xiong and Li affirm that since the contact points are on the offset profile of the workpiece, they can use objective function formulated as a least squares problem (Xiong 2003). Lin and Sun investigated the stylus tip radius correction using the multi-cross-product method (Lin and Sun 2003). Another approach for stylus tip radius correction has been based on the use of the part CAD model. Some techniques rely on building a parametric surface or contours followed by the creation of an offset surface using the least square method (Jeong and Kim 1999). Liang and Lin developed a point data conversion algorithm to find the estimated surface normal vector at every point without reconstruction of the surface model (Liang and Lin 2002). They connect surrounding points and on this basis formulate triangular meshes directly from the dense data points set, thus as to determine the normal vector of each point for stylus tip radius correction. Park et al. proposed a probe with an internal elastic structure fitted with strain gauges so that the contact force between the tip and the measured surface can be estimate and used for the calculation of the stylus tip correction vector (Park, Kwon et al. 2006). Aoyama et al. proposed a potentiometric spherical tip capable of detecting the point of contact with an electrically conducting object surface (Aoyama, Kawai et al. 1989).

Without going into details of the case of freeform surfaces, the purpose of this section is to describe the technical implementation of error compensation in case of areas sections of a known geometric primitive such as a plane, circle, sphere, cone, torus, etc., analyzing the effects of such implementation on MScMS-II. With MScMS-II, this correction is negligible if using a sharp tip. This type of probe, however, has several drawbacks that limit its use:

-it is not able to make measurements approaching the piece sideways;
-it may introduce a geometrical error due to the imperfections of the tip;
-it introduces a risk of damage to the object to be measured.

4.1. *Implementation*

From the practical point of view, the procedure implemented for MScMS-II follows the following steps:

1. Specification of the target geometry. During this phase the system user is asked to specify the geometry of the surface to be measured;
2. Measurement. In this phase a certain number of points P'_i are acquired by means of the portable probe.
3. Reconstruction of the envelop. Knowing the specified geometry of the surface, the system computes the envelop interpolating the points P'_i.
4. Calculation of the touched points. Knowing the radius of the tip of the probe, the position of the center of the probe P'_i and the surface normal $\vec{n}_i$, the generic contact point P_i can be obtained through the relation:

$$P_i = P'_i \pm \vec{n}_i \cdot \rho \qquad (4)$$

The operator sign depends on the direction of approach of the probe.

As an example, consider the simple case of estimating a two-dimensional geometry: a circumference. When measuring a circumference, the envelop of points corresponds to another circle, with the same center but different radius (see Fig. 8). The radius depends on the measurement procedure: if the measurement is made approaching the circumference from the outside (outside diameter) the radius will be greater than the real one and vice versa if the measurement is made from within (inside diameter).

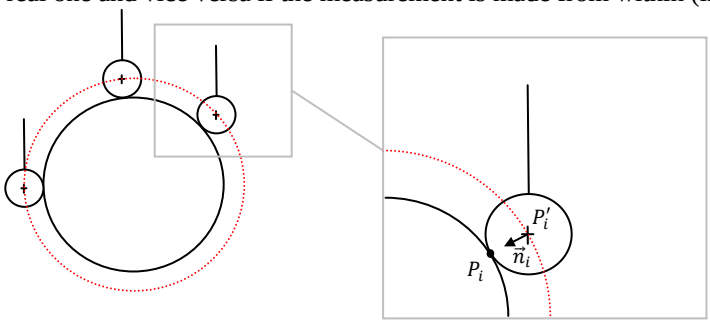

Figure 8. A schematization of the stylus tip approach to a circumference. The dotted line represents the envelop of the points measured by the CMM which, in the particular case, corresponds to a circumference with a different radius.

During the third step of the procedure described above, the system is able to calculate the geometry of the envelop points P'_i. Being a circumference, the radius ρ' and the center x_0 of the envelop are calculated.

So far, for each point of the envelop, the normal vector can be calculated as:

$$\vec{n} = \frac{x_0 - P_i}{\rho} \qquad (5)$$

Knowing the normal vector, the contact points P_i can be easily calculated as:

$$P_i = P_i' \pm \vec{n}_i \cdot \rho \qquad (6)$$

Note the sign of equation (6). In this example it must be choosen positive, it would have been negative in case of a measurement made with the probe approaching the circumference from the inside.

4.2. *Test*

To make explicit the extent of the improvement deriving from the implementation of the correction model described above, the following test was thought. A section of a cylinder calibrated with a CMM (DEA Iota0101) was measured with the MScMS-II. The measure was repeated 30 times in different locations within the working volume of MScMS-II (Peggs, Maropoulos et al. 2009).

The results of the measurements with and without correction model were compared with each other (see Fig. 9). The nominal value of the radius of the cylinder section was obtained by calibration.

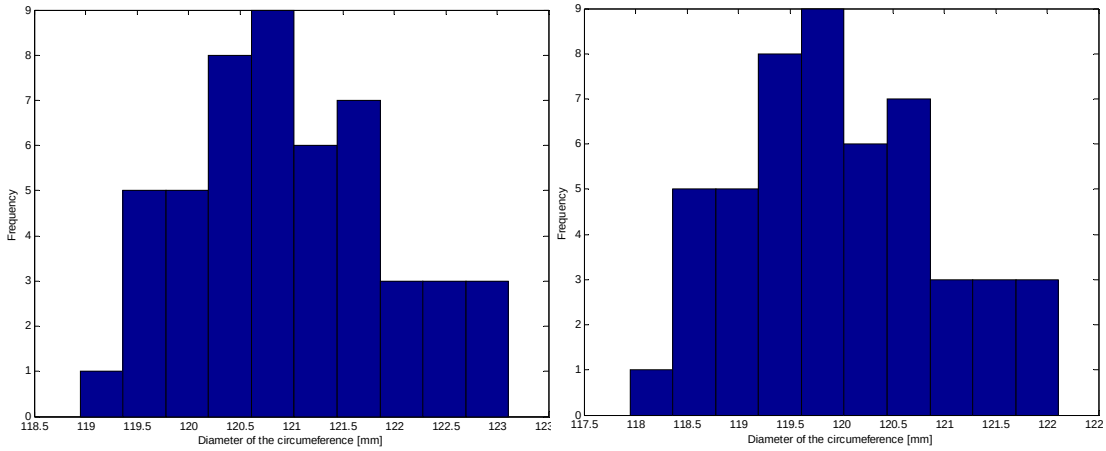

Figure 9. Results of the measurement of the diameter of a cylinder section with (a) and without (b) the tip radius correction.

If compared to the nominal value of the diameter of the cylinder section ($d = 120.00$ mm), the results presented in Fig. 9 show a bias in the measurement of $b = 0.98$ mm that, as expected, is about half the size of the tip of MScMS-II probe (2 mm). This bias reduces to 0.02 mm when the measurement is corrected considering the size of the probe tip.

5. Bias due to the kinematic of the probe

One of the most well-known and often-used mathematical tools used for stochastic estimation from noisy sensor measurements is the Kalman filter. The Kalman filter is named after Rudolph E. Kalman, who, in 1960, published his famous paper describing a recursive solution to the discrete-data linear filtering problem (Kalman 1960). The Kalman filter is essentially a set of mathematical equations that implement a predictor-corrector type estimator that is optimal in the sense that it minimizes the estimated error covariance—when some presumed conditions are met (Kalman 1960). One of the assumptions for the application of the Kalman filter is the knowledge of the measurement process.

5.1. *The measuring process with MScMS-II*

When measuring using the MScMS-II, the operator has to bring the probe in contact with the object being measured. At this point, he presses the trigger to take measurements. Although fast enough, this operation is not instantaneous. At a time when the trigger is pressed, the system collects a sample of measurement replications for a fraction of a second (less than one third of a second). During this period, the position of the tip of the probe is supposed to be stationary. For this reasons, the equations that describe this process are:

$$x_k = x_{k-1} + s_k \qquad (7)$$

with a measurement $z \in \mathbb{R}^3$ that is

$$z_k = x_k + t_k \qquad (8)$$

where $x_k \in \mathbb{R}^3$ is the position of the probe tip at time k and the random variables $s_k \in \mathbb{R}^3$ and $t_k \in \mathbb{R}^3$ represent the process and measurement noise. They are assumed to be independent (of each other), white, and with normal probability distributions:

$$\begin{matrix} p(s) \sim \mathcal{N}_3(0, Q) \\ p(t) \sim \mathcal{N}_3(0, R) \end{matrix} \qquad (9)$$

Q and R are respectively the process noise covariance and the measurement noise covariance matrices. Although they could potentially vary in time, they are assumed to be constant in time.

5.2. *The filter equation parameters*

The time update equations are

$$\begin{matrix} \hat{x}_k^- = \hat{x}_{k-1}^- \\ P_k^- = P_{k-1}^- + Q \end{matrix} \qquad (10)$$

where P_k^- and P_{k-1}^- are respectively the *a priori* estimates of error covariance at time step *k* and *k-1* and $\hat{x}_k^-$ and $\hat{x}_{k-1}^-$ are respectively the *a priori* state estimates at time step *k* and *k-1*.

On the other hand, the measurement update equations are

$$\begin{aligned} K_k &= P_k^-(P_k^- + R)^{-1} \\ \hat{x}_k &= \hat{x}_k^- + K_k(z_k - \hat{x}_k^-) \\ P_k &= (1 - K_k)P_k^- \end{aligned} \qquad (11)$$

where P_k is the *a posteriori* estimate of error covariance, $\hat{x}_k$ is the a posteriori state estimate at time step k, K_k is the gain that minimizes the *a posteriori* error covariance at step k (Welch and Bishop 1995). Presuming a very small process variance, it is possible to assume

$$Q = \begin{pmatrix} 1e^{-5} & 0 & 0 \\ 0 & 1e^{-5} & 0 \\ 0 & 0 & 1e^{-5} \end{pmatrix} \qquad (12)$$

Assuming a small but non-zero value for Q gives more flexibility in "tuning" the filter (Kalman 1960; Welch and Bishop 1995). The filter is "seed" with the guess $\hat{x}_{k-1}^- = x_0$. Similarly the initial value for P_{k-1}, call it P_0 is set as

$$P_0 = \begin{pmatrix} 1 & 0 & 0 \\ 0 & 1 & 0 \\ 0 & 0 & 1 \end{pmatrix} \qquad (13)$$

Basing on preliminary empirical tests of measurement accuracy reported by Galetto, Mastrogiacomo et al. (2010), the measurement error variance is fixed at

$$R = \begin{pmatrix} 1 & 0 & 0 \\ 0 & 1 & 0 \\ 0 & 0 & 1 \end{pmatrix}. \qquad (14)$$

5.3. *Test*

In order to provide an idea of the effect of the implementation of this filter, a simple test was designed. In normal operation conditions, the measurement of the position of the probe tip is the result of the acquisition of approximately thirty repetitions of measurement. The system, in fact, has a capture rate that ensures, under these assumptions, an acquisition time of less than 3 tenths of a second. During this period the operator is supposed to keep the probe tip reasonably still.

To give evidence of the effect of the implementation of the filter, 300 repetitions of measurement were recorded keeping the probe still for about 3 seconds. Fig. 10 shows, on the same graph, the measurement with and without the implementation of the filter.

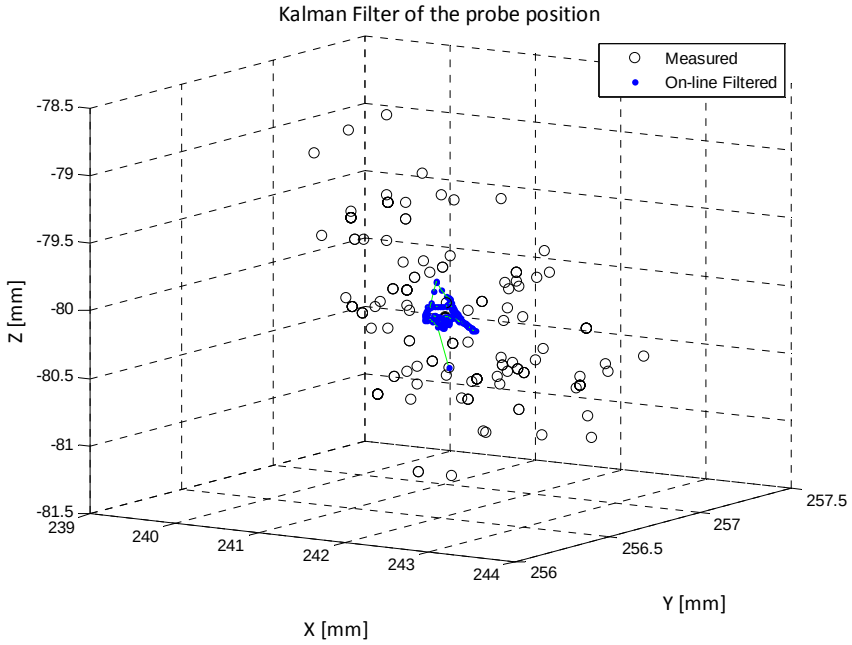

Figure 10. Example of application of the Kalman filter.

From the plot, there is evidence of the fact that the filtered measurements are much more stable than the unfiltered ones. Considering the first 30 observations, the variability of filtered data is respectively $\sigma_x = 0.07$, $\sigma_x = 0.04$ mm and $\sigma_z = 0.09$ mm. On the other hand, the variability of unfiltered data is respectively $\sigma_x = 0.35$ mm, $\sigma_x = 0.13$ mm and $\sigma_z = 0.29$ mm.

6. Conclusions and future developments

This work stems from the need to address three open problems in the development of MScMS-II: the error due to lens distortion and the bias due to both the physical size of the probe and its kinematic.

The correction algorithms herein presented are derived from the literature and adapted to MScMS-II. The novelty of this paper lies in the adaptation and application of methods to the prototype. These aspects are not trivial for a system that is far from classical metrology systems from the point of view of the architecture and working principles.

Although the paper addresses the issues in depth with satisfactory results, this study opens several research scenarios for the improvement of the system. As regards the model of lens distortion, a thorough study should be carried out in order to investigate the contributions of the various terms of the polynomial correction. The questions, in this case would be: “In what order is it worth truncating the polynomial development of the model? And which are the effects of the calibration procedure on the calculation of

the coefficients of the polynomial?". Furthermore an analysis of possible correlations between the major error contributors could be necessary in order to demonstrate the completeness of achieved corrections.

On the other hand, the study of the kinematics of the probe led to the introduction of the Kalman filter to filter the noise that the instrument introduces to the static measurement. The natural extension of the model to the cinematic case has still to be considered and analyzed.

7. References

1. Aoyama, H., M. Kawai, et al. (1989). "A new method for detecting the contact point between a touch probe and a surface." CIRP Annals-Manufacturing Technology **38**(1): 517-520.
2. Bar-Shalom, Y., X. R. Li, et al. (2001). Estimation with applications to tracking and navigation, Wiley Online Library.
3. Brown, D. C. (1971). "Close-range camera calibration." Photogrammetric engineering **37**(8): 855-866.
4. Franceschini, F., M. Galetto, et al. (2011). Distributed Large Scale Dimensional Metrology: New Insights. London, UK, Springer.
5. Galetto, M., L. Mastrogiacomo, et al. (2010). "The Mobile Spatial coordinate Measuring System II (MScMS-II): system description and preliminary assessment of the measurement uncertainty." International Journal of Metrology and Quality Engineering **1**(2): 111-119.
6. Galetto, M., L. Mastrogiacomo, et al. (2010). "A wireless sensor network-based approach to large-scale dimensional metrology." International Journal of Computer Integrated Manufacturing **23**(12): 1082-1094.
7. Galetto, M., L. Mastrogiacomo, et al. (2011). "MScMS-II: an innovative IR-based indoor coordinate measuring system for large-scale metrology applications." International Journal of Advanced Manufacturing Technology **52**(1-4): 291-302.
8. Hocken, R. J. and P. H. Pereira, Eds. (2012). Coordinate Measuring Machines and Systems, CRC Press.
9. Jeong, J. and K. Kim (1999). "Generation of tool paths for machining free-form pockets with islands using distance maps." The International Journal of Advanced Manufacturing Technology **15**(5): 311-316.
10. Kalman, R. E. (1960). "A new approach to linear filtering and prediction problems." Journal of basic Engineering **82**(1): 35-45.
11. Lee, J. C. (2008). "Hacking the nintendo wii remote." IEEE Pervasive Computing: 39-45.
12. Liang, S. R. and A. C. Lin (2002). "Probe-radius compensation for 3D data points in reverse engineering." Computers in Industry **48**(3): 241-251.
13. Lin, Y. and W. Sun (2003). "Probe radius compensated by the multi-cross product method in freeform surface measurement with touch trigger probe CMM." The International Journal of Advanced Manufacturing Technology **21**(10): 902-909.
14. Luhmann, T., S. Robson, et al. (2006). Close range photogrammetry: principles, techniques and applications, Whittles.

15. Mayer, J., Y. Mir, et al. (1997). "Touch probe radius compensation for coordinate measurement using kriging interpolation." Proceedings of the Institution of Mechanical Engineers, Part B: Journal of Engineering Manufacture **211**(1): 11.
16. Park, J., K. Kwon, et al. (2006). "Development of a coordinate measuring machine (CMM) touch probe using a multi-axis force sensor." Measurement Science and Technology **17**: 2380.
17. Peggs, G., P. G. Maropoulos, et al. (2009). "Recent developments in large-scale dimensional metrology." Proceedings of the Institution of Mechanical Engineers, Part B: Journal of Engineering Manufacture **223**(6): 571-595.
18. Song, C. K. and S. W. Kim (1997). "Reverse engineering: autonomous digitization of free-formed surfaces on a CNC coordinate measuring machine." International Journal of Machine Tools and Manufacture **37**(7): 1041-1051.
19. Welch, G. and G. Bishop (1995). "An introduction to the Kalman filter." University of North Carolina at Chapel Hill, Chapel Hill, NC **7**(1).
20. Wozniak, A., J. R. R. Mayer, et al. (2009). "Stylus tip envelop method: corrected measured point determination in high definition coordinate metrology." The International Journal of Advanced Manufacturing Technology **42**(5): 505-514.
21. Xiong, Z. (2003). "Probe radius compensation of workpiece localization." Journal of manufacturing science and engineering **125**: 100.
22. Zhang, Z. (1999). Flexible camera calibration by viewing a plane from unknown orientations, Ieee.
23. Zhongwei, Y., Z. Yuping, et al. (2003). "Methodology of NURBS surface fitting based on off-line software compensation for errors of a CMM." Precision engineering **27**(3): 299-303.